Input–Output Linearization of a Boost Converter With Mixed Load (Constant Voltage Load and Constant Power Load)

Sameer Arora, *Student Member, IEEE*, Poras Balsara, *Fellow, IEEE*, and Dinesh Bhatia, *Senior Member, IEEE*

***Abstract*—Power converters and electric motor drives when tightly regulated behave as constant power loads. These loads are different from resistive loads and have destabilizing negative impedance characteristics, which impact a system's stability. A boost converter is intrinsically nonlinear and is a nonminimum phase system at the output voltage with respect to the control input. The linear approximation of this boost converter loaded with a constant power load has a zero and poles in the right half of the s-plane, making the system unstable and very difficult to control. Control techniques that employ some form of system inversion cannot be implemented for a nonminimum phase system. This paper describes a technique to modify the nonminimum phase boost converter to a minimum phase for a constant power load, further implementing the input–output linearization technique to stabilize the system. This paper also provides a methodological analysis of the problem followed by the proposed solution. Furthermore, it verifies the analysis of the proposed solution through simulation and experimental results.**

***Index Terms*—Boost converter, cascaded system, constant power load (CPL), dc–dc, input–output linearization (IOL), nonlinear control, right half-plane (RHP) zero, right half-plane (RHP) pole, wide operating range.**

NOMENCLATURE

S	Steady state represented by an uppercase letter.
$\hat{s}$	Small signal represented by lowercase with hat.
s	Signal represented by a lowercase letter.
u	Control input.
y	Output variable.
$f(x)$	System vector of a nonlinear system.
$g(x)$	Control input vector of a nonlinear system.
$h(x)$	Output of a nonlinear system.
$L_f h(x)$	Lie derivative of the output vector along the system trajectory $f(x)$ i.e., $f(x)\frac{\partial h(x)}{\partial x}$.
n	Order of the system.
r	Relative degree (defined as $L_g L_f^{(r-1)} h(x) \neq 0$).
x_1	System state representing inductor current.
x_2	System state representing capacitor voltage.

Manuscript received October 3, 2017; revised January 1, 2018; accepted February 23, 2018. Date of publication March 8, 2018; date of current version November 19, 2018. Recommended for publication by Associate Editor M. Ordonez. *(Corresponding author: Sameer Arora.)*

The authors are with the Erik Jonsson School of Engineering and Computer Science, University of Texas, Dallas, TX 75080 USA (e-mail:

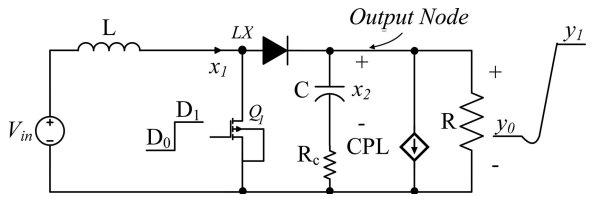

Fig. 1. Boost converter with a combination of a resistive load in parallel with a CPL [33]. A dip in the output voltage is observed for a step change in the duty cycle ($D_0 \rightarrow D_1$) because of unstable zero dynamics.

and they make the system very bulky and is a concern with space and footprint on a printed circuit board (PCB) [2], [9], [11], [12].

Another method to tackle the CPL problem is by active damping. In [13], an active damping control technique is proposed, which emulates a virtual resistance in parallel to the CPL. In [17], the authors propose an active damping method by adding compensating current to the CPL modifying the control structure for a point-of-load converter such that a virtual capacitor is added to a CPL power reference. However, these CPL-side active damping methods affect the power quality of the CPL. Other CPL-side active damping methods can be found in [14]–[16] and [32]. Active damping method as in [32] stabilizes the CPL using a supercapacitor and in [14] by using a concept of an active power filter.

The boost converter is a nonminimum phase system because of the indirect transfer of energy between the inductor and the output capacitor. This phenomenon can be explained using the boost converter operating with the duty cycle D, as shown in Fig. 1. In the steady state, the inductor is charged during the ON-time instant of the switch and discharged to charge the capacitor during the OFF-time instant of the switch. For a step increase in the duty cycle from D_0 to D_1 of a boost converter in a closed loop, the switch (Q_1) remains ON for a longer time storing more energy in the inductor, whereas the output capacitor is starved of energy. Due to this, the control action sees the decrease of the output voltage (y_0), thereby increasing the duty cycle to make the effect worse. This causes the voltage across the capacitor to drop momentarily resulting in a dip in the output voltage before it starts to increase and ramp to the final output voltage (y_1). The voltage across the capacitor starts to ramp up when there is enough energy built up in the inductor. The time taken for the capacitor voltage and, therefore, the output voltage to increase after the step duty is applied gives the measure of the right half-plane (RHP) zero in the control-to-output transfer function. A capacitor that takes a longer time to recover implies a lower frequency zero. For high-bandwidth systems, this momentary dip in the output may cause the system to become unstable. Therefore, the crossover frequency of the closed-loop system is restricted to about one-fifth of the RHP zero frequency.

Passivity-based control solutions for a boost converter considering the load dynamics to be a purely CPL are found in [25] and [26]. The passivity-based controller obtained is in the form of a nonlinear inverse quadratic proportional–derivative (PD) controller [24], [25]. The major disadvantage of passivity-based control is that it can only be implemented for a system that is at least a weakly minimum phase system and has a relative degree equal to one [34]. The authors in [25] state that the proposed passivity-based controller has stability limitations as the boost converter has unstable internal dynamics. Furthermore, the PD-derived controller poses a noise susceptibility issue. Another method as proposed in [26] implements passivity-based control with interconnection. The disadvantage of this implementation is that it is designed for one operating point of the CPL [28]. Overall, passivity-based control has poor noise immunity due to the presence of differentiator and is sluggish in response [28].

Other nonlinear control methods such as sliding-mode control, synergetic-based control, current-mode control, and model-predictive control can be found in [2], [21], [22], and [27]. Sliding-mode control due to simple implementation and robustness has wide applications. It has been used for stabilizing dc–dc converters and mitigating CPL-based instabilities [6], [23], [28]. The major disadvantage of sliding-mode control is chattering and the variable switching frequency that can have an effect on the filtering requirement of the boost converter. Additionally, sliding-mode control is an inversion control technique, which requires the internal dynamics to be stable. Synergetic-based control is implemented in [21] and has a disadvantage of being highly sensitive to high-frequency noise. Current-mode control has been studied in [2], where the stability of the system is analyzed in a small-signal sense. Model-predictive control has also been studied to stabilize multiconverter systems feeding CPLs and is a relatively new ground for researchers, and many problems are yet to be addressed thoroughly [27].

Feedback linearization is classified as an active damping method where feedback is used to actively damp the nonlinearity of the CPL [2]. Theoretically, feedback linearization can compensate any amount of CPL and stabilize the system in a large-signal sense [9], [28]. Feedback linearization is generally based on finding a nonlinear feedback, which when applied cancels the nonlinearity. Consequently, linear control tools can be applied to design the controller [6]. Implementation of feedback linearization is restricted to nonminimum phase systems but can be implemented for a nonminimum phase boost converter by bypassing the minimum phase requirement by applying an input state rather that input–output linearization (IOL) [35]. The major disadvantage of input-state linearization is that it is not suitable for output tracking control unless there is a way to express the desired states in terms of the output trajectory. Another method to control the nonminimum phase boost converter is to regulate the output voltage by indirectly regulating the inductor current [36]. The problem with indirect regulation is that the system is unable to shape the output response. The output voltage response evolves according to the open-loop dynamics, resulting in a slower response and overshoot/undershoot. Additionally, the system is very sensitive to circuit parameters and load variations [37], [38]. Another way to regulate the nonminimum phase system is to redefine the output such that the system with respect to the redefined output is a minimum phase system [39]. In [40], an output redefinition method is implemented to control the boost converter by exact linearization. A linear combination of the inductor current and the output current is redefined as the output of the system to obtain a minimum phase system. The major disadvantage is that the system has a considerable

output voltage error in the steady state. Additionally, during the calculation of the reference current, the exact value of the load resistance is required, which can be a variable parameter, and implementation for the CPL might be more complex. Furthermore, the system is prone to cross minimum-to-nonminimum phase boundaries during transients and might share the same shortcoming as for indirect voltage regulation.

Active damping methods using feedback linearization were demonstrated in [9] using a loop-cancellation technique and in [10] using voltage-mode control. The implementation in [9] requires a reciprocal block that is difficult to implement and a differentiator block that is highly sensitive to noise. Furthermore, the technique adds another state to system modeling, thereby increasing system complexity. The authors in [10] use an active damping method to establish the small-signal stability. The solutions presented in [9] and [10] do not alter the internal dynamics; therefore, the system would be band limited and will result in a slower response. Other works using feedback linearization are discussed in [9], [41], and [42]. In [9] and [41], the buck dc–dc converter is stabilized for a combination load of a CPL and a resistive load. In [42], the authors implement feedback linearization using a coordinate transform for a pure CPL with a full-order feedback controller.

The instability issues posed by the CPL has lead researchers to investigate the problem extensively. Overall, there is no general solution, and more research needs to be done in this field. Depending on the design requirements, a suitable CPL compensation technique may be chosen. The figure of merit to evaluate the performance of a stabilizing technique is based on the amount of CPL the technique can compensate, robustness, dynamic response, immunity to noise, and large-signal stability. Theoretically, the feedback linearization technique can compensate any amount of CPL and achieve large-signal stability [9], [28]. Furthermore, feedback linearization has been reported to have good stability and transient characteristics [43]. These advantages offered by feedback linearization are motivating enough for IOL to be the choice for the control law.

IOL cannot be applied to systems with unstable zero dynamics. The use of the inversion control law like IOL offers an advantage of the simple extension to the nonlinear setting. Additionally, the fact that the output chosen determines the zero dynamics, it is suitable to define the output to make the system a minimum phase or a weakly minimum phase. The proposed method is based on output redefinition presented in [44]. This technique makes the system a minimum phase system by *injecting small-signal inductor current at the output node, while the output voltage is sampled during the* OFF*-time instance of the switch*. Furthermore, the proposed control method does not use derivative or reciprocal blocks; therefore, higher immunity to noise and wider operating range can be achieved.

The rest of this paper is organized as follows. Section II discusses the boost converter's nonlinear model, its control dynamics, and its stability issues. Section III discusses a method to stabilize the zero dynamics to modify the linear approximation to render it a minimum phase system. This paper gives consideration to the nonlinear model for analysis and uses the linear approximation just to locally stabilize the zero dynamics of the system. In Section IV, IOL is implemented for the modified system. Section V presents the simulation and experimental results for the closed-loop system. Also, for the experimental verification of the proposed algorithm, a practical implementation of a CPL was implemented. Finally, contributions and summary are given in Section VI.

II. Boost Converter Nonlinear Model

This section discusses the control dynamics and stability issues related to the nonlinear model of a boost converter with the CPL. Consideration is given to the large-signal model of the system, where there is no limitation on the signal swing. Additionally, for a multiconverter distributed power system, the load conditions do not exist purely as a CPL; therefore, the boost converter is modeled here (in Fig. 1) with a combination of a CPL and a resistive load.

Neglecting the value of the output capacitor equivalent series resistance (ESR) (R_c), the ordinary differential equations for the boost converter, as shown in Fig. 1, are given by

$$\begin{cases} \dot{x_1} = \frac{V_{\text{in}}}{L} - \frac{x_2}{L}(1-d) \\ \dot{x_2} = \frac{x_1}{C}(1-d) - \frac{x_2}{RC} - \frac{P}{x_2 C} \\ y = x_2 \end{cases} \tag{1}$$

where V_{in} is the input voltage, and x_1 and x_2 are states of the system representing inductor (L) current and capacitor (C) voltage, respectively. R is the resistive load and P is the CPL. Here, the control input u of the generalized nonlinear system is represented by the duty cycle d.

A. Control Dynamics

The control dynamics of the system can be studied to understand the stability of the control variable (d) when the system is in the steady state. Differentiating the second equation of (1) and substituting x_1 and $\dot{x_1}$, the input–output relation of the boost converter is given as

$$\ddot{x}_2 + \dot{x}_2\left[\frac{\dot{d}}{(1-d)} + \frac{1}{RC} - \frac{P}{x_2^2 C}\right] + x_2\left[\frac{(1-d)^2}{LC} + \frac{\dot{d}}{RC(1-d)} + \frac{\dot{d}P}{x_2^2(1-d)}\right] = \frac{V_{\text{in}}(1-d)}{LC}. \tag{2}$$

At zero dynamics $x_2 = X_{20} \Rightarrow \dot{x}_2 = 0$, $\ddot{x}_2 = 0$, the input–output relation is given as

$$\dot{d} = \frac{(1-D)^2}{LCX_{20}\left[\frac{1}{RC} + \frac{P}{X_{20}^2}\right]}\left[V_{\text{in}} - X_{20}(1-D)\right]. \tag{3}$$

For the stable operating condition under the steady state, $\dot{d} = 0$. Fig. 2 shows the phase portrait for control dynamics (3) for different duty ratios (10%, 20%, ... 70%, 80%). It demonstrates that control dynamics (3) has two equilibrium points at $D = 1$ and $D = 1 - V_{\text{in}}/X_{20}$, where the former is a partially stable operating point and the latter is an unstable operating point, as seen in Fig. 2 with diverging trajectories [38].

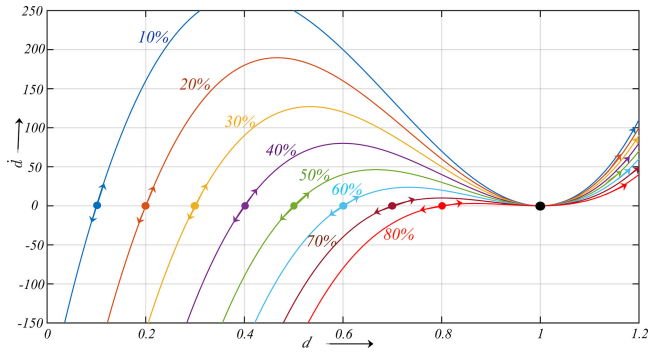

Fig. 2. Phase portrait of the input dynamics showing the zero dynamics unstable due to diverging trajectories near the equilibrium point of interest ($\dot{d} = 0$) for duty cycles 10%, 20%, ... 70%, and 80% for a boost converter with parameter values of $L = 100\,\mu$H, $C = 100\,\mu$F, $V_{\text{in}} = 12$ V, $P = 8$ W, and $R = 50\,\Omega$.

As observed in Fig. 2, the control dynamics is unbounded at the equilibrium point of interest. Thus, inversion control techniques such as IOL cannot be applied for the boost converter under the following conditions.

B. Stability

The CPL exhibits a positive instantaneous impedance but a negative incremental impedance. This means that although the instantaneous impedance $(\frac{V}{I} > 0)$ of the CPL is positive, the delta change in the impedance $(\frac{\Delta V}{\Delta I} < 0)$ is negative, which can have an effect on the stability of the system. The instability of negative impedance can be explained with a simple example. Consider a general second-order system whose characteristic equation is given as

$$s^2 + 2\alpha s + {\omega_o}^2 = 0 \tag{4}$$

where the roots are given as

$$\begin{cases} s_1 = -\alpha + \sqrt{\alpha^2 - {\omega_o}^2} \\ s_2 = -\alpha - \sqrt{\alpha^2 - {\omega_o}^2}. \end{cases} \tag{5}$$

The characteristic equation of the second-order RLC system is in the form of

$$s^2 + s\frac{R}{L} + \frac{1}{LC} = 0 \tag{6}$$

or

$$s^2 + s\frac{1}{RC} + \frac{1}{LC} = 0 \tag{7}$$

where α known as the damping factor can be $R/2L$ or $1/2RC$.

For a CPL, the small-signal resistance (R) is negative; therefore, as implied by (5), the roots of the system will have poles in the RHP, making the system unstable. It is important to note that negative impedance does not mean that the physical value of the resistance is negative. It means that unlike a resistance whose phase shift and magnitude gain is zero and one, respectively, a negative resistance phase shift and magnitude gain is 180° and 1, respectively. A negative resistance in a closed loop would have a total phase shift of 360°, i.e., a positive feedback. This is because negative feedback contributes 180° phase shift and a negative resistance would contribute an additional 180°, making a total phase shift of 360°.

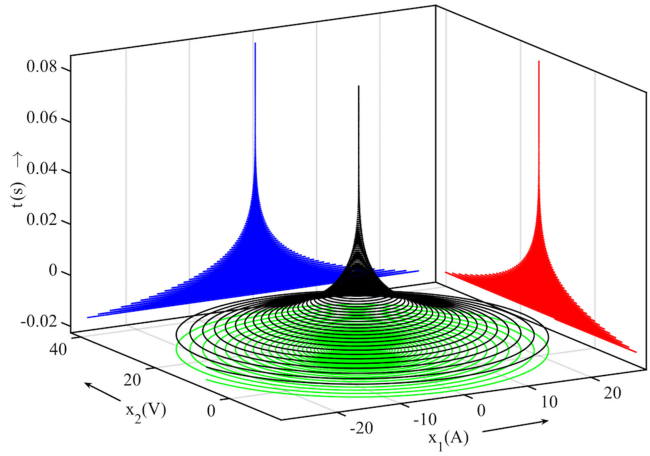

Fig. 3. System trajectory for a boost converter with a stable orbit ($L = 100\,\mu$H, $C = 100\,\mu$F, $D = 0.2$, $V_{\text{in}} = 12$ V, $R = 50\,\Omega$, and $P_{\text{CPL}} = 0$ W). *Note:* Blue and red represent signals evolved over time, green represents phase portrait, and black represents system trajectory.

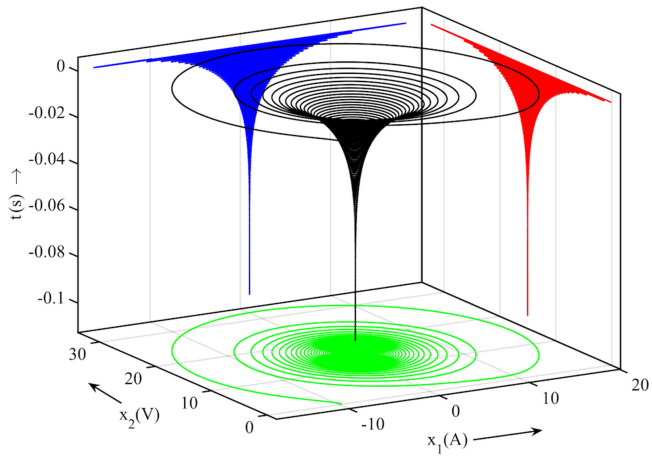

Fig. 4. System trajectory for a boost converter with an unstable orbit ($L = 100\,\mu$H, $C = 100\,\mu$F, $D = 0.2$, $V_{\text{in}} = 12$ V, $R = 50\,\Omega$, and $P_{\text{CPL}} = 8$ W). *Note:* Blue and red represent signals evolved over time, green represents phase portrait, and black represents system trajectory.

Based on the above idea, the stability of the boost converter with a mixed load of CPL and a resistive load can be analyzed by studying the phase portrait of the boost converter. For a given operating point ($D = 0.2$), Figs. 3–5 show the composite plots of the boost converter (1) in an open loop with parameter values of $L = 100\,\mu$H, $C = 100\,\mu$F, $D = 0.2$, $V_{\text{in}} = 12$ V, $R = 50\,\Omega$ and CPL power (P_{CPL}) varied between 0 to 8 W. The state variables (x_1, x_2) and time (t) are represented on the three axes. Figs. 3 and 4 show the system trajectory (in black) evolving over time to a stable orbit for the condition resistive power $(P_R = V^2/R = \frac{V_{\text{in}}^2}{(1-D)^2 R} = 4.5$ W) greater than the CPL power ($P_{\text{CPL}} = 0$ W) and an unstable trajectory for the CPL power ($P_{\text{CPL}} = 8$ W) greater than the resistive power $(P_R = V^2/R = \frac{V_{\text{in}}^2}{(1-D)^2 R} = 4.5$ W), respectively. Fig. 5

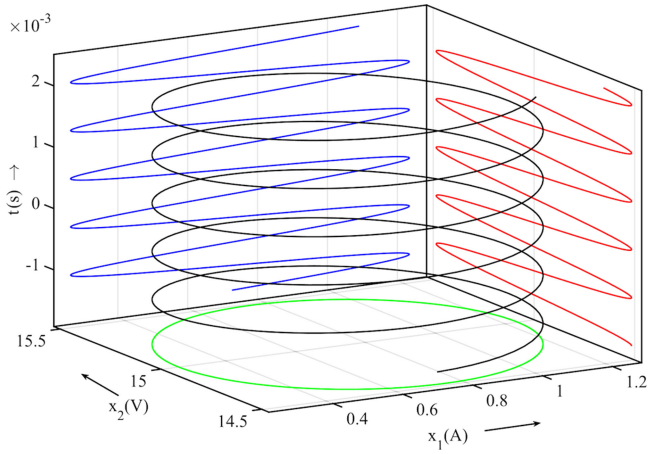

Fig. 5. Limit cycle for the boost converter for the CPL power ($P_{\rm CPL}$) equal to the resistive power (P_R) ($L = 100\,\mu$H, $C = 100\,\mu$F, $D = 0.2$, $P = 4.5$ W, and $R = 50\,\Omega$). *Note:* Blue and red represent signals evolved over time, green represents phase portrait, and black represents system trajectory.

TABLE I
CHANGE IN EIGENVALUES AND SYSTEM STABILITY FOR THE BOOST CONVERTER WITH $V_{\rm in} = 12$ V, CPL $= 8$ W, $R = 50\,\Omega$, $L = 100\,\mu$H, AND $C = 100\,\mu$F AS A FUNCTION OF DIFFERENT OPERATING POINTS (DUTY RATIOS)

Duty	Eigenvalues	Stability	Eq. pt. (X_{10}, X_{20})
10%	$20.8333 \pm j3674.1755$	Unstable	0.96296,13.33
20%	$12.962 \pm j3265.9606$	Unstable	1.0417, 15
30%	$6.0185 \pm j2857.7317$	Unstable	1.1565,17.14
40%	$-8.52e^{-7} \pm j2857.73$	Limit Cycle	1.3333, 20
50%	$-5.09259 \pm j2041.235$	Stable	1.6267, 24
60%	$-9.25925 \pm j1632.966$	Stable	2.1667, 30
70%	$-12.5 \pm j1224.6811$	Stable	3.333, 40
80%	$-14.81481 \pm j816.3622$	Stable	6.667, 60

considers the case when the CPL power is equal to the resistive power ($D = 0.2$, $P = 4.5$ W, and $R = 50\,\Omega$), a limit cycle is observed. Here, the system has imaginary eigenvalues.

Table I summarizes the behavior of a boost converter with $V_{\rm in} = 12$ V, CPL $= 8$ W, $R = 50\,\Omega$, $L = 100\,\mu$H, and $C = 100\,\mu$F for different duty cycles (D). From the table, it is clear how the eigenvalues and, therefore, the system's stability change with the change in duty ratio (D).

From the above analysis, it has been proven that the system, as well as its internal dynamics, is not well behaved. Furthermore, it is found that the stability is a function of the loading condition (CPL) and the operating point (D) for a given CPL.

III. PROPOSED METHOD

IOL [34], [39], [45] is an active damping feedback linearization technique and can be used to stabilize dc–dc converters with a CPL. The implementation of IOL is such that the control is fed back into the system such that a linear map between the input and the output is obtained canceling the nonlinearities. However, IOL is a type of inversion control technique, in which its implementation requires some form of system inversion. It is, therefore, critical that the zero of the system be in the left half plane (LHP), else the inversion control law would contain an RHP pole, which is not a feasible design.

To implement the proposed control law, consider the following definition.

Definition: The fixed point p of a nonlinear system is hyperbolic if and only if the Jacobian $\frac{\partial f}{\partial x}(p)$ has no critical eigenvalues, i.e., no eigenvalue with zero real part [45].

The Hartman–Grobman theorem states that the orbit structure of a dynamical system in a neighborhood of a hyperbolic equilibrium point (as defined in the definition) is topologically equivalent to the orbit structure of the linearized dynamical system. Thus, modifying the zero dynamics of the linear approximation, the overall zero dynamics of the nonlinear system is modified.

The zero dynamics of the system can be modified by three methods: changing the output variable, modifying the plant itself, or changing the system trajectory [39]. Assuming no input feedforward, intuitively, we can say that for a linear system defined by $A, B, \tilde{C}, \tilde{D}$ matrices,[1] the A matrix determines stability, the B matrix shifts the origin of the system to the steady-state value, and A and $\tilde{C}$ play a role in determining the stability of the zero dynamics [39], [45].

Therefore, redefining the $\tilde{C}$ matrix of the linear approximation, the qualitative behavior of the zero dynamics of the nonlinear system can be changed around the neighborhood of the equilibrium point to render the system minimum phase [46]. It has been demonstrated in [33] and [47]–[49] that by sampling the output voltage during the OFF-time instant of the switch, the $\tilde{C}$ matrix of the system is modified (change of the output variable). The zero in the RHP of the boost converter moves to the left half when the inequality condition

$$R_c C > \frac{L}{R(1-D)} \tag{8}$$

is met.

To further elaborate this point relative to our problem, we discuss the linear model of the boost converter when loaded with the CPL in the following section.

A. Linear Model of a Boost Converter With a CPL

Using Taylor series linearization, the linear state-space model of a boost converter, as shown in Fig. 1, sampled during OFF-time about an operating point (X_{10}, X_{20}, D), is given by

$$A = \begin{bmatrix} -\frac{(1-D)RR_c}{(R+R_c)L} & -\frac{(1-D)R}{(R+R_c)L} - \frac{P}{X_{20}^2}\frac{RR_c(1-D)}{(R+R_c)L} \\ \frac{(1-D)R}{C(R+R_c)} & -\frac{1}{(R+R_c)C} + \frac{P}{X_{20}^2 C}\frac{R}{(R+R_c)} \end{bmatrix}$$

$$B = \begin{bmatrix} \frac{X_{10}RR_c}{L(R+R_c)} + \frac{X_{20}R}{L(R+R_c)} - \frac{RR_cP}{LX_{20}(R+R_c)} \\ -\frac{R}{(R+R_c)}\frac{X_{10}}{C} \end{bmatrix}$$

$$\tilde{C} = \begin{bmatrix} \frac{RR_c}{(R+R_c)} & \frac{P(RR_c)}{(R+R_c)} + \frac{R}{(R+R_c)} \end{bmatrix}$$

$$\tilde{D} = 0. \tag{9}$$

[1]The feedforward matrix is represented as $\tilde{D}$ to differentiate between the steady-state duty cycle D, and the output matrix is represented as $\tilde{C}$ to differentiate between the capacitor value C.

Implementing a multilayer ceramic capacitor, R_c can be approximated as $R_c << R \Rightarrow (R + R_c) \approx R$, $R_c^2 \approx 0$. Thus, the overall control to output transfer function can be reduced to

$$\frac{\hat{y}}{\hat{d}} = \frac{1}{\Delta(s)}\left[s\left(\frac{R_c X_{20}}{L} - \frac{PR_c X_{10}}{X_{20}^2 C} - \frac{X_{10}}{C}\right) + \frac{(1-D)R_c X_{10}}{LC} + \frac{R_c X_{20}}{RLC} - \frac{PR_c}{X_{20}LC} + \frac{X_{20}(1-D)}{LC}\right] \tag{10}$$

where

$$\Delta(s) = s^2 + s\left(\frac{1}{RC} - \frac{P}{X_{20}^2 C} + \frac{(1-D)R_c}{L}\right) + \frac{(1-D)R_c}{RLC} + \frac{(1-D)^2}{LC}. \tag{11}$$

The steady-state values are given by

$$X_{10} = \frac{V_{\text{in}}}{(1-D)^2 R} + \frac{P}{V_{\text{in}}}$$
$$X_{20} = \frac{V_{\text{in}}}{(1-D)}. \tag{12}$$

Substituting the steady-state values (12) into (10), for the system's zero to be in the LHP, the terms associated with s in the numerator of (10) must meet the following inequality:

$$R_c C > \frac{P(1-D)L}{V_{\text{in}}^2} + \frac{L}{R(1-D)}. \tag{13}$$

Furthermore, from the terms associated with s in the denominator of (10), it can be concluded that the system has complex RHP poles for the condition

$$P > \frac{X_{20}^2}{R} + \frac{(1-D)R_c C}{LX_{20}^2}. \tag{14}$$

Therefore, the boost converter is a nonminimum phase if condition (13) is not met and unstable for the condition in (14). It is interesting to note that this translates to the discussion, as presented in Section II, where the nonlinear boost converter had unstable control dynamics and was unstable when the CPL is greater than that of the resistive load (also implied by the Hartman–Grobman theorem).

B. Stabilizing the Zero Dynamics by Current Injection

Consider the output node of the boost converter shown in Fig. 1. During the OFF-time instant of the switch (Q_1), the dc portion of the inductor current flows to the output load and the ac current flows through the capacitor, which is in series with the ESR (R_c) of the capacitor. The output voltage is given by the voltage developed across the ESR (R_c) and the capacitor voltage. The transfer function at the output (w.r.t. control input d) would be a linear combination of the transfer function of the capacitor voltage (w.r.t. control input d) and the transfer function of the inductor current (w.r.t. control input d) weighted by the ESR (R_c) of the capacitor. The transfer function of the inductor current (w.r.t. control input d) has zero in the LHP. Using inductor current information that rides on the ESR (R_c), the dip in the output voltage can be obscured by increasing the ESR (R_c) of the capacitor, thereby to move the zero in the LHP. Mathematically, this is represented by inequality condition (13). However, increasing the ESR (R_c) causes a large ripple at the output voltage and loss of efficiency, as well as huge thermal stress on the output capacitor. Alternatively, inductor current injection can be used to emulate the ESR (R_c) of the capacitor and alleviate the dependence on the ESR of the capacitor when using the OFF-time sampling instant of the switch. Adding a small ac inductor current (scaled by a small factor Q) to the output voltage results in a virtual resistor in series with the output capacitor. Thus, by manipulating this factor (Q), the unstable zero dynamics of the system can be converted to stable zero dynamics with smaller ripple and better efficiency [44].

Under the assumption mentioned in Section III-A, from (9), the output matrix of the boost converter is given as $\tilde{C} = [R_c \quad PR_c/X_{20}^2 + 1]$. Adding inductor current (by a factor Q), the redefined output matrix $\tilde{C}$ can now be defined as $\tilde{C}_{\text{new}} = [(Q + R_c) \quad PR_c/X_{20}^2 + 1]$. The transmission zero of the linearized system can be calculated [50] from

$$\det\begin{bmatrix} sI - A & B \\ -\tilde{C} & \tilde{D} \end{bmatrix} = \det\begin{bmatrix} s & \frac{1-D}{L} & \frac{X_{20}}{L} \\ -\frac{1-D}{C} & s + \frac{1}{RC} - \frac{P}{X_{20}^2 C} & -\frac{X_{10}}{C} \\ -(Q + R_c) & -PR_c/X_{20}^2 - 1 & 0 \end{bmatrix} = 0 \tag{15}$$

$$s\left[\frac{X_{20}(Q+R_c)}{L} - \frac{X_{10}}{C} - \frac{PR_c X_{10}}{X_{20}^2}\right] + (Q + R_c)\left[\frac{X_{10}(1-D)}{LC} + \frac{X_{20}}{RLC} - \frac{P}{LCX_{20}}\right] + \frac{X_{20}(1-D)}{LC} + \frac{PR_c(1-D)}{LCX_{20}} = 0. \tag{16}$$

Substituting steady-state values (12) into (16), for the system's zero to be in the LHP, the terms associated with s in (16)

$$\left[\frac{X_{20}(Q+R_c)}{L} - \frac{X_{10}}{C} - \frac{PR_c X_{10}}{X_{20}^2}\right] \tag{17}$$

needs to meet the following inequality:

$$(Q + R_c)C > \frac{P(1-D)L}{V_{\text{in}}^2} + \frac{L}{R(1-D)}. \tag{18}$$

This method of stabilization of zero dynamics for the system locally near the operating point renders the overall system a minimum phase. It is important to note that the inductor current injected at the output node is a small-signal leading to the linear model of approximation being used. The current injection does not affect the large-signal behavior of the system. Furthermore, based on inequality (18), the virtual current injection factor (Q) can be designed for the worst case. Overall, the output redefinition implementation offers multiple advantages such as the following:

1) simpler implementation;
2) very small steady-state error, since it modifies the small-signal behavior;

3) once the zero is stabilized for the worst case, the system would not cross boundaries between the minimum phase and the nonminimum phase during transients;
4) output redefinition still facilitates regulation of the output variable of interest.

This technique allows us to implement the IOL control technique, which is discussed in the following section.

IV. Input–Output Linearization

IOL has long been established in the nonlinear control system literature [34], [39], [45]. To implement IOL on a single-input single-output nonlinear system, the output (y) of the system is differentiated until the control input (u) appears in the resulting equation. The number of times the output is differentiated is equal to the relative degree (r). When applying a coordinate transform, the dynamics of a nonlinear system can be decomposed into its external linear subsystem (input–output of r dimension) and its internal subsystem ($n-r$ dimension unobservable). Here, "n" represents the order of the system. The linear subsystem is stabilized with linear state feedback control. The dynamics of the unobservable subsystem represents the internal dynamics and is called zero dynamics when the states of the linear subsystem are at rest [34], [39], [45].

By IOL, a linear differential relation between the output y and the auxiliary control input ν is generated. IOL cannot be implemented for an unstable system with unstable internal dynamics as for the case of the boost converter with a CPL. However, by stabilizing the internal dynamics, as discussed in Section III-B, IOL can be implemented at least locally, canceling the nonlinearities and transforming the system into a linear one.

Differentiating the redefined output ($y=(R_c+Q)x_1+x_2$) till the relative degree ($r=1$) and using the differential equation (1) of the boost converter ($n=2$), the duty cycle d can be calculated as

$$d=\frac{1}{\gamma(x_1,x_2)}\Bigg[-(R_c+Q)CV_{\text{in}}+(R_c+Q)Cx_2-(R_cP+1)\times Lx_1+(R_cP+1)L\left(\frac{x_2}{R}+\frac{P}{x_2}\right)-kLC(x_2-X_{20})\Bigg] \tag{19}$$

where

$$\gamma(x_1,x_2)=(R_c+Q)Cx_2-(R_cP+1)Lx_1. \tag{20}$$

Equation (19) forms the control law for the system where a proportional controller is implemented with the gain k. Fig. 6 shows the complete block diagram for the implementation of the proposed method. The overall loop gain $T(s)$ of the system (as shown in Fig. 6) linearized around the operating point (X_{10},X_{20}) is given as

$$T(s)=\frac{\hat{d}}{\hat{v}}\times\frac{\hat{y}}{\hat{d}}\times k=\frac{k}{s} \tag{21}$$

where $\hat{d}/\hat{v}$ is the inverse transfer function because of IOL implementation. Therefore, the closed-loop transfer function of the system is given as

$$\frac{T(s)}{1+T(s)}=\frac{k}{s+k} \tag{22}$$

where, auxiliary control input $v=-k(y-y_0)$.

IOL is applicable for a nonlinear system for the condition that the zero dynamics of the system are asymptotically stable [39], [45]. After applying IOL for the boost converter, the linear part of the nonlinear system has all the poles in the open LHP resulting in the linear part of the system to be asymptotically stable. Therefore, by the implication of definition discussed in Section III, the resulting nonlinear system is asymptotically stable and small parameter variation of L and C in (19) and higher order unmodeled dynamics will not upset the local asymptotic stability. IOL can be applied to many applications and has been generalized as tracking inverters in [51].

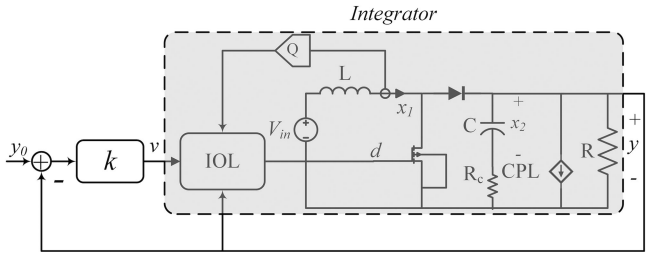

Fig. 6. Implementation of the closed-loop boost converter with IOL with a proportional controller. The shaded portion of the block diagram is represented as an integrator due to IOL implementation, i.e., $\dot{y}=\text{V}$, where $v=k(y-Y_o)$.

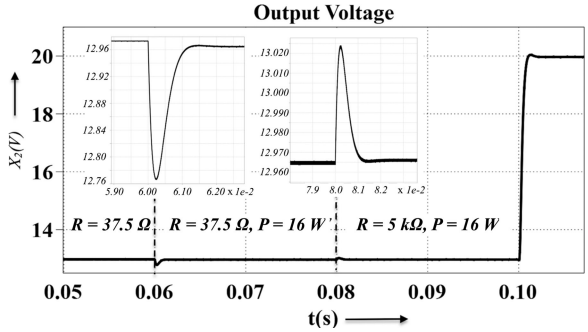

Fig. 7. Simulation of the boost converter under various load conditions. The boost converter is subjected to a resistive load of 37.5 Ω, a combination load of 37.5 Ω, and 16-W CPL and an approximately pure CPL (16-W CPL and 5 kΩ). Furthermore, the system is subjected to a step response for a step change of 13 to 20 V for a combination load of 16-W CPL and 5 kΩ.

V. Simulation and Experimental Results

Simulation results for boost converter ($L=100\,\mu$H, $C=600\,\mu$F, $f_s=100$ kHz, $k=2000$, $Q=0.2$, and $f_{\text{sample}}=100$ kHz (off-time instant)) were obtained using PLECS block set over Simulink. The controller was simulated using the IOL control technique with OFF-time sampling. The simulation results are shown in Fig. 7. During startup, the boost converter is subjected to a resistive load of 37.5 Ω with the capacitor initial voltage equal to 13 V. At time = 0.06 s, the boost converter is subjected to a combination load of 37.5 Ω and 16-W CPL,

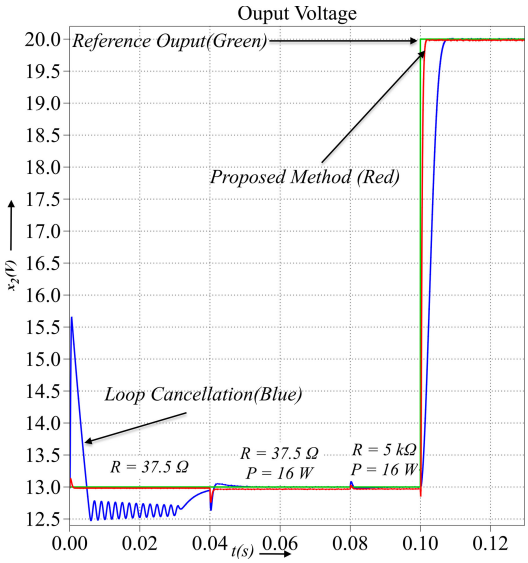

Fig. 8. Comparison between the loop cancellation technique [9] (shown in blue) and the proposed method (shown in red). The proposed method offers a better transient response, better tracking, no overshoot/undershoot, and does not exhibit ringing during startup.

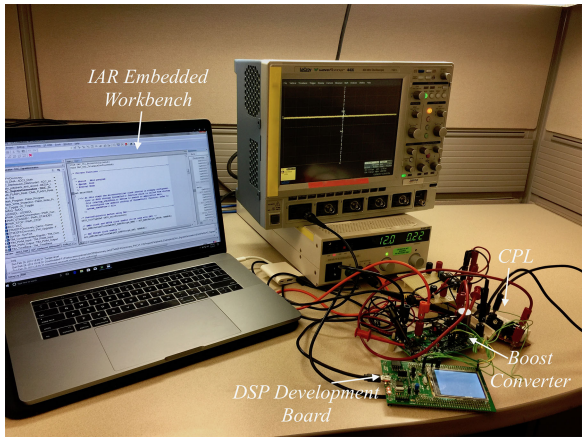

Fig. 9. Experimental setup for the closed-loop boost converter loaded with a CPL. Shown in the diagram is the DSP development board interfaced to IAR embedded workbench communicating over USB cable, a CPL [52], and the boost converter.

where an undershoot of 21 mV is observed at the output voltage. At time = 0.08 s, the boost converter is subjected to approximately pure CPL (16-W CPL and 5 k Ω) to which an overshoot of 60 mV is observed at the output. Additionally, the system is subjected to a step change of 13 to 20 V in the output reference at time = 0.1 s for a combination load of 16-W CPL and 5 k Ω. The simulation results prove that proposed technique works and demonstrates that the boost converter implementing the proposed output redefinition and control technique can regulate the boost converter with constant voltage load and/or CPL. As discussed in Section IV, the relative degree of the system is 1, and on applying IOL, the input–output map of the system would be approximated as a single integrator. The load regulation and the step response of the boost converter under proportional control, as seen in Fig. 7, verify it to be a single pole response.

This paper implements output redefinition in conjunction with OFF-time sampling to stabilize the zero dynamics. Furthermore, as the implemented output redefinition method stabilizes the zero dynamics, input–output feedback linearization is used to obtain a linear input to output map. The proposed method can be compared to a previous work implementing the input-state feedback linearization technique. Fig. 8 shows the comparison simulation results between the loop cancellation technique [9] and the proposed method for the same system parameters, initial conditions, and loading conditions. The figure demonstrates the superiority of the proposed method. The proposed method offers a better transient response, better tracking, no overshoot/undershoot, and does not exhibit ringing during the startup. However, an observation of a few millivolt error is observed during the steady state when the boost converter is loaded with a CPL of 16 W and a resistive load of 37.5 Ω. This is because the feedback observes the output voltage when sampled during the OFF-time instant, which is average output voltage plus half of the ripple voltage due to ESR (R_c), where ripple voltage changes with loading conditions. Overall, the closed-loop system is not band limited because of stabilization of the zero (as seen by the controller); therefore, the crossover frequency can be designed for the one-fifth of the switching frequency, than otherwise would be one-tenth RHP zero; therefore, a faster time response can be achieved.

To experimentally validate the proposed method, a CPL was implemented [52]. The implemented CPL has a much faster response rate than the response time of a dc–dc converter ensuring CPL operation. The CPL implementation has an error of $\leq 1\%$ with a response time of $\approx 2.5\ \mu$s [52].

Fig. 9 shows the experimental setup for the system. Shown in the diagram is the DSP development board interfaced to IAR embedded workbench communicating over a USB cable, the implemented CPL [52], and the boost converter implemented on a PCB. The circuit elements of the boost converter are as follows: inductor $L = 100\ \mu$H, output capacitor $C = 604\ \mu$F, the estimated ESR of the output capacitor $R_c = 0.25$ m Ω, power MOSFET (Infineon IPP80N06S207) and power diode (Vishay MBR745-E3/45), input voltage $V_{\text{in}} = 12$ V, switching frequency $f_s = 100$ kHz, and output sampled during OFF-time instant ($f_{\text{sampling}} = 100$ kHz). The system was tested with a load resistor and CPL values ranged from $R = 37.5\ \Omega$ to 5 k Ω and 0 to 16 W, respectively. The proposed control technique was implemented using the ARM-based DSP processor development board, STM32F429-discovery.

Fig. 10 shows the closed-loop system response of the boost converter with a CPL of 16 W and a resistor of 5 k Ω when the output voltage reference was changed from 13 to 20 V. The output voltage is sampled during the OFF-time instant of the switch, which is the same as the switching frequency (100 kHz). The plot shows the output voltage (red), the output current (green), and the CPL (blue) that remains constant during the step change in the output voltage reference. The results obtained are similar to simulation results obtained for the step change in the reference voltage.

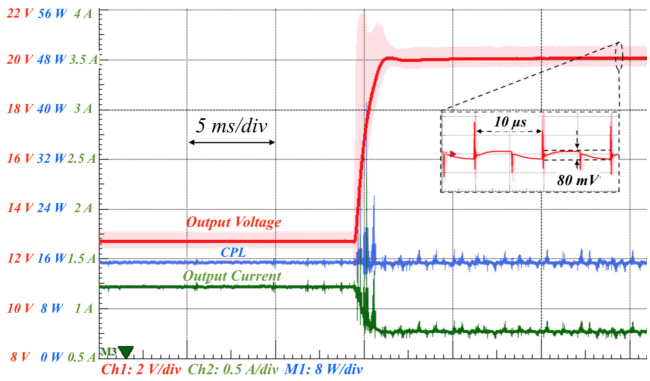

Fig. 10. Step change in reference from 13 to 20 V for a boost converter when loaded by a 16-W CPL and a 5 kΩ resistance. The output voltage is sampled during the OFF-time instant of the switch, which is the same as the switching frequency (100 kHz).

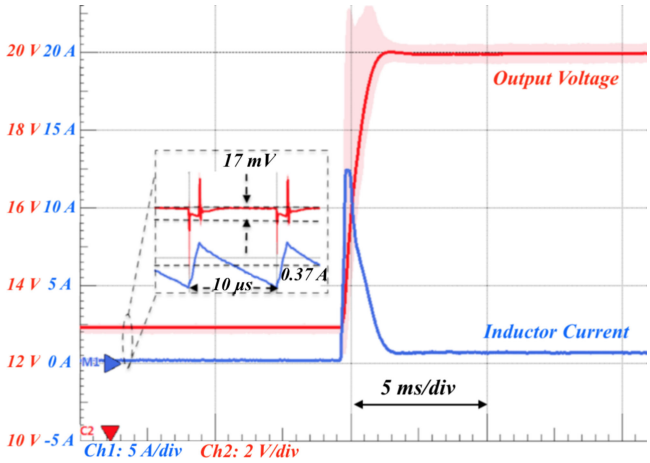

Fig. 11. Step response of the boost converter for a 37.5 Ω resistive load for a reference step change from 13 to 20 V. The output voltage is sampled during the OFF-time instant of the switch, which is the same as the switching frequency (100 kHz).

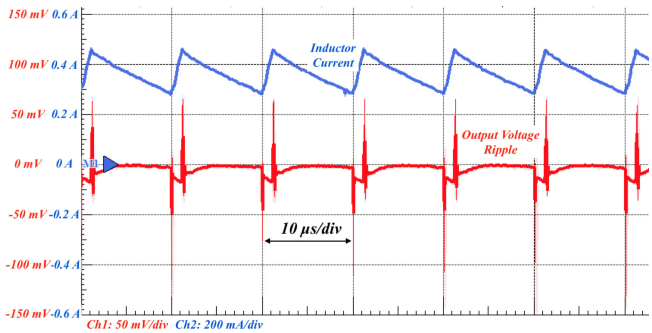

Fig. 12. Output voltage ripple (red) and inductor current waveforms (blue) for a boost converter for a 37.5 Ω resistive load at 13 V. An output voltage ripple of 17 mV and an average inductor current of 0.37 A are observed. A spike in the output voltage is observed due to the resonance between the parasitic capacitance and the stray inductance present at the LX node of the boost converter (see Fig. 1).

Fig. 11 shows the closed-loop system response of the boost converter with a 37.5Ω resistor load when the output voltage reference was changed from 13 to 20 V. Figs. 12 and 13 show the inductor current and the output ripple for the boost converter when loaded by a 37.5 Ω resistor at 13 and 20 V, respectively.

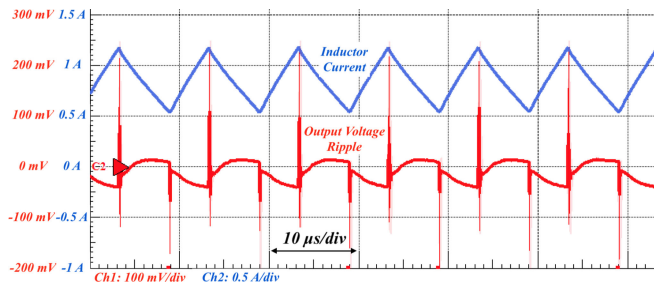

Fig. 13. Output voltage ripple (red) and inductor current waveforms (blue) for a boost converter for a 37.5 Ω resistive load at 20 V. An output voltage ripple of 56 mV and an average inductor current of 0.85 A are observed. A spike in the output voltage is observed due to the resonance between the parasitic capacitance and the stray inductance present at the LX node of the boost converter (see Fig. 1).

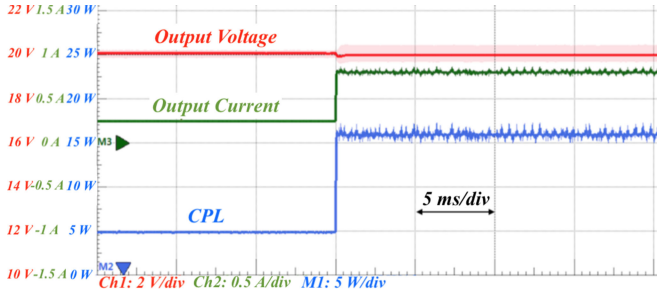

Fig. 14. Closed-loop behavior of the boost converter for a step change in the CPL from 5 to 16 W at 20 V. The figure shows the output voltage (red), the output current (green), and the subjected CPL (blue).

An average inductor current value of 0.37 A with an output voltage ripple of 17 mV is seen at 13 V, and an average inductor current value of 0.85 A with output voltage ripple of 56 mV at 20 V was observed. A spike in the output voltage during a switching event is observed due to the resonance between the parasitic capacitance and the stray inductance present at the LX node of the boost converter (see Fig. 1). Furthermore, as shown in Figs. 10 and 11, a dip in the output voltage during the step change in reference is observed. This is due to the intrinsic zero of the boost converter present on the averaged output voltage waveform (an oscilloscope shows the average output voltage). This dip in the output voltage with the current injection technique would not be observed by the controller when the output voltage is observed during the OFF-time instant of the switch.

Fig. 14 shows the closed-loop system behavior of the boost converter loaded by a 5 kΩ resistor and the CPL is dynamically changed from 5 to 16 W ($<2.5\ \mu$s) at an output voltage of 20 V. The figure shows the load regulation, where the output voltage is represented in red, the output current in green, and the CPL in blue. Overall, the experimental results conform with the simulation results. Additionally, the system shows a similar response to CPL or resistive load corresponding with the analysis and highlighting the advantage of the IOL technique.

VI. Contributions and Summary

This paper proposes and demonstrates a control technique for a nonlinear boost converter with a combination of a CPL and

a resistive load. The proposed method implements the output redefinition method to dampen the internal dynamics and IOL to dampen the system dynamics by canceling nonlinearities due to the CPL. The proposed technique offers multiple advantages compared to the existing control techniques.

1) The proposed closed-loop design achieves an overall single-pole response independent of loading conditions (CPL and/or resistive load) with no overshoot/undershoot.
2) It regulates variable of interest.
3) Since the internal dynamics are stable, the system is not band limited and a faster controller can be designed.
4) A linear map between the input and the output facilitates very good tracking control.
5) It has a wider dynamic range and better noise immunity.
6) It is independent of the operating point.
7) Small variations in the parameter values do not disturb the local asymptotic stability.
8) The linear subsystem and unobservable internal dynamics are stable.

Overall, an efficient performance is achieved at all feasible operating points with larger dynamic range. The proposed method can be generalized and can be extended to other dc–dc converters, which show nonminimum phase characteristics such as the buck–boost converter and the flyback converter.

REFERENCES

[1] A. Rahimi and A. Emadi, "An analytical investigation of dc/dc power electronic converters with constant power loads in vehicular power systems," *IEEE Trans. Veh. Technol.*, vol. 58, no. 6, pp. 2689–2702, Jul. 2009.

[2] Y. Li, K. R. Vannorsdel, A. J. Zirger, M. Norris, and D. Maksimovic, "Current mode control for boost converters with constant power loads," *IEEE Trans. Circuits Syst. I, Reg. Papers*, vol. 59, no. 1, pp. 198–206, Jan. 2012.

[3] A. Khaligh, S. Williamson, and A. Emadi, "Control and stabilization of dc/dc buck-boost converters loaded by constant power loads in vehicular systems using a novel digital scheme," in *Proc. 12th Int. Power Electron. Motion Control Conf.*, Aug. 2006, pp. 1769–1775.

[4] A. Rahimi, A. Khaligh, and A. Emadi, "Design and implementation of an analog constant power load for studying cascaded converters," in *Proc. 32nd Annu. Conf. IEEE Ind. Electron. Soc.*, Nov. 2006, pp. 1709–1714.

[5] Z. Gao, X. Zhang, and H. Lin, "Modeling and nonlinear control for the boost converter with constant power loads," in *Proc. Asia-Pacific Power Energy Eng. Conf.*, Mar. 2010, pp. 1–4.

[6] A. Emadi, A. Khaligh, C. Rivetta, and G. Williamson, "Constant power loads and negative impedance instability in automotive systems: Definition, modeling, stability, and control of power electronic converters and motor drives," *IEEE Trans. Veh. Technol.*, vol. 55, no. 4, pp. 1112–1125, Jul. 2006.

[7] S. Kim and S. S. Williamson, "Negative impedance instability compensation in more electric aircraft dc power systems using state space pole placement control," in *Proc. IEEE Veh. Power Propulsion Conf.*, Sep. 2011, pp. 1–6.

[8] G. Sulligoi, D. Bosich, G. Giadrossi, L. Zhu, M. Cupelli, and A. Monti, "Multiconverter medium voltage dc power systems on ships: Constant-power loads instability solution using linearization via state feedback control," *IEEE Trans. Smart Grid*, vol. 5, no. 5, pp. 2543–2552, Sep. 2014.

[9] A. Rahimi, G. Williamson, and A. Emadi, "Loop-cancellation technique: A novel nonlinear feedback to overcome the destabilizing effect of constant-power loads," *IEEE Trans. Veh. Technol.*, vol. 59, no. 2, pp. 650–661, Feb. 2010.

[10] A. Rahimi and A. Emadi, "Active damping in dc/dc power electronic converters: A novel method to overcome the problems of constant power loads," *IEEE Trans. Ind. Electron.*, vol. 56, no. 5, pp. 1428–1439, May 2009.

[11] M. Cespedes, L. Xing, and J. Sun, "Constant-power load system stabilization by passive damping," *IEEE Trans. Power Electron.*, vol. 26, no. 7, pp. 1832–1836, Jul. 2011.

[12] F. Gao, S. Bozhko, S. Yeoh, G. Asher, and P. Wheeler, "Stability of multi-source droop-controlled electrical power system for more-electric aircraft," in *Proc. IEEE Int. Conf. Intell. Energy Power Syst.*, Jun. 2014, pp. 122–126.

[13] M. Wu and D. D. C. Lu, "A novel stabilization method of LC input filter with constant power loads without load performance compromise in dc microgrids," *IEEE Trans. Ind. Electron.*, vol. 62, no. 7, pp. 4552–4562, Jul. 2015.

[14] Q. Shafiee, T. Dragicevic, J. C. Vasquez, and J. M. Guerrero, "Modeling, stability analysis and active stabilization of multiple dc-microgrid clusters," in *Proc. IEEE Int. Energy Conf.*, May 2014, pp. 1284–1290.

[15] P. Magne, B. Nahid-Mobarakeh, and S. Pierfederici, "General active global stabilization of multiloads dc-power networks," *IEEE Trans. Power Electron.*, vol. 27, no. 4, pp. 1788–1798, Apr. 2012.

[16] P. Magne, B. Nahid-Mobarakeh, and S. Pierfederici, "Active stabilization of dc microgrids without remote sensors for more electric aircraft," *IEEE Trans. Ind. Appl.*, vol. 49, no. 5, pp. 2352–2360, Sep./Oct. 2013.

[17] P. Magne, D. Marx, B. Nahid-Mobarakeh, and S. Pierfederici, "Large-signal stabilization of a dc-link supplying a constant power load using a virtual capacitor: Impact on the domain of attraction," *IEEE Trans. Ind. Appl.*, vol. 48, no. 3, pp. 878–887, May/Jun. 2012.

[18] M. Wu and D. D. C. Lu, "An active damping method for stabilization of cascaded connected two stage converter systems with constant power loads in dc microgrids," in *Proc. IEEE Int. Symp. Circuits Syst.*, Jun. 2014, pp. 2664–2667.

[19] A. Khaligh, A. M. Rahimi, and A. Emadi, "Modified pulse-adjustment technique to control dc/dc converters driving variable constant-power loads," *IEEE Trans. Ind. Electron.*, vol. 55, no. 3, pp. 1133–1146, Mar. 2008.

[20] A. Khaligh, A. M. Rahimi, and A. Emadi, "Negative impedance stabilizing pulse adjustment control technique for dc/dc converters operating in discontinuous conduction mode and driving constant power loads," *IEEE Trans. Veh. Technol.*, vol. 56, no. 4, pp. 2005–2016, Jul. 2007.

[21] E. Santi, D. Li, A. Monti, and A. M. Stankovic, "A geometric approach to large-signal stability of switching converters under sliding mode control and synergetic control," in *Proc. IEEE 36th Power Electron. Spec. Conf.*, Jun. 2005, pp. 1389–1395.

[22] I. Kondratiev, E. Santi, R. Dougal, and G. Veselov, "Synergetic control for dc-dc buck converters with constant power load," in *Proc. IEEE 35th Annu. Power Electron. Spec. Conf.*, Jun. 2004, vol. 5, pp. 3758–3764.

[23] Y. Zhao, W. Qiao, and D. Ha, "A sliding-mode duty-ratio controller for dc/dc buck converters with constant power loads," *IEEE Trans. Ind. Appl.*, vol. 50, no. 2, pp. 1448–1458, Mar./Apr. 2014.

[24] A. Kwasinski and C. N. Onwuchekwa, "Dynamic behavior and stabilization of dc microgrids with instantaneous constant-power loads," *IEEE Trans. Power Electron.*, vol. 26, no. 3, pp. 822–834, Mar. 2011.

[25] A. Kwasinski and P. T. Krein, "Stabilization of constant power loads in dc-dc converters using passivity-based control," in *Proc. 29th Int. Telecommun. Energy Conf.*, Sep. 2007, pp. 867–874.

[26] J. Zeng, Z. Zhang, and W. Qiao, "An interconnection and damping assignment passivity-based controller for a dc-dc boost converter with a constant power load," *IEEE Trans. Ind. Appl.*, vol. 50, no. 4, pp. 2314–2322, Jul./Aug. 2014.

[27] H. Mahmoudi, M. Aleenejad, and R. Ahmadi, "A new modulated model predictive control method for mitigation of effects of constant power loads," in *Proc. IEEE Power Energy Conf. Illinois*, Feb. 2016, pp. 1–5.

[28] S. Singh, A. R. Gautam, and D. Fulwani, "Constant power loads and their effects in DC distributed power systems: A review," *Renew. Sustain. Energy Rev.*, vol. 72, pp. 407–421, 2017. [Online]. Available: http://www.sciencedirect.com/science/article/pii/S1364032117300412

[29] L. Herrera, W. Zhang, and J. Wang, "Stability analysis and controller design of dc microgrids with constant power loads," *IEEE Trans. Smart Grid*, vol. 8, no. 2, pp. 881–888, Mar. 2017.

[30] R. Haroun, A. E. Aroudi, A. Cid-Pastor, and L. Martinez-Salamero, "Stability issues in cascade connected switching converters for dc microgrid applications," in *Proc. IEEE Int. Symp. Circuits Syst.*, May 2013, pp. 1324–1327.

[31] R. Erickson and D. Maksimovic, *Fundamentals of Power Electronics* (ser. Power Electronics). New York, NY, USA: Springer, 2001. [Online]. Available: https://books.google.com/books?id=On9-rJTR8ygC

[32] X. Chang, Y. Li, X. Li, and X. Chen, "An active damping method based on a supercapacitor energy storage system to overcome the destabilizing effect of instantaneous constant power loads in dc microgrids," *IEEE Trans. Energy Convers.*, vol. 32, no. 1, pp. 36–47, Mar. 2017.
[33] S. Arora, P. T. Balsara, and D. K. Bhatia, "Effect of sampling time and sampling instant on the frequency response of a boost converter," in *Proc. 42nd Annu. Conf. IEEE Ind. Electron. Soc.*, Oct. 2016, pp. 7155–7160.
[34] C. Byrnes, A. Isidori, and J. Willems, "Passivity, feedback equivalence, and the global stabilization of minimum phase nonlinear systems," *IEEE Trans. Autom. Control*, vol. 36, no. 11, pp. 1228–1240, Nov. 1991.
[35] H. A. Talebi, R. V. Patel, and K. Khorasani, *Control of Flexible-Link Manipulators Using Neural Networks*, vol. 261. New York, NY, USA: Springer, 2001.
[36] H. Sira-Ramirez and R. Ortega, "Passivity-based controllers for the stabilization of dc-to-dc power converters," in *Proc. 34th IEEE Conf. Decision Control*, Dec. 1995, vol. 4, pp. 3471–3476.
[37] G. Escobar, R. Ortega, H. Sira-Ramirez, J. Vilain, and I. Zein, "An experimental comparison of several nonlinear controllers for power converters," *IEEE Control Syst.*, vol. 19, no. 1, pp. 66–82, Feb. 1999.
[38] R. Ortega, J. A. L. Perez, P. J. Nicklasson, and H. Sira-Ramirez, *Passivity-Based Control of Euler-Lagrange Systems: Mechanical, Electrical and Electromechanical Applications*. New York, NY, USA: Springer, 2013.
[39] J.-J. E. Slotine *et al.*, *Applied Nonlinear Control*, vol. 199. Englewood Cliffs, NJ, USA: Prentice-Hall, 1991.
[40] Y. M. Roshan and M. Moallem, "Control of nonminimum phase load current in a boost converter using output redefinition," *IEEE Trans. Power Electron.*, vol. 29, no. 9, pp. 5054–5062, Sep. 2014.
[41] A. Emadi and M. Ehsani, "Negative impedance stabilizing controls for PWM dc-dc converters using feedback linearization techniques," in *Proc. 35th Intersoc. Energy Convers. Eng. Conf. Exhibit.*, 2000, vol. 1, pp. 613–620.
[42] J. A. Solsona, S. G. Jorge, and C. A. Busada, "Nonlinear control of a buck converter which feeds a constant power load," *IEEE Trans. Power Electron.*, vol. 30, no. 12, pp. 7193–7201, Dec. 2015.
[43] J. Zhou and X. Lu, "Review of exact linearization method applied to power electronics system," in *Proc. Asia-Pacific Power Energy Eng. Conf.*, Mar. 2012, pp. 1–4.
[44] R. Taylor, L. Hunt, and V. Paduvalli, "System and method for controlling output ripple of dc-dc converters with leading edge modulation control using current injection," U.S. Patent 13/720 850, Jun. 20, 2013. [Online]. Available: http://www.google.com/patents/US20130154586
[45] H. K. Khalil and J. Grizzle, *Nonlinear Systems*, vol. 3, Englewood Cliffs, NJ, USA: Prentice-Hall, 1996.
[46] J. Bao and P. L. Lee, *Process Control: The Passive Systems Approach* (ser. Advances in Industrial Control). New York, NY, USA: Springer, 2007.
[47] V. Yousefzadeh, M. Shirazi, and D. Maksimovic, "Minimum phase response in digitally controlled boost and flyback converters," in *Proc. 22nd Annu. IEEE Appl. Power Electron. Conf.*, Feb. 2007, pp. 865–870.
[48] S. Arora, P. Balsara, D. Bhatia, R. Taylor, and B. Hunt, "Gain and phase (GAP) measurement device," in *Proc. IEEE Appl. Power Electron. Conf. Expo.*, Mar. 2015, pp. 2453–2458.
[49] D. M. Sable, B. H. Cho, and R. B. Ridley, "Use of leading-edge modulation to transform boost and flyback converters into minimum-phase-zero systems," *IEEE Trans. Power Electron.*, vol. 6, no. 4, pp. 704–711, Oct. 1991.
[50] C.-T. Chen, *Linear System Theory and Design*. Oxford, U.K.: Oxford Univ. Press, 1995.
[51] L. Hunt, "Tracking converters with input output linearization control," WO Patent App. PCT/US2013/049 879, Mar. 6, 2014. [Online]. Available: https://www.google.ch/patents/WO2014011738A3?cl=en
[52] S. Arora, P. T. Balsara, and D. K. Bhatia, "Digital implementation of constant power load (CPL), active resistive load, constant current load and combinations," in *Proc. IEEE Dallas Circuits Syst. Conf.*, Oct. 2016, pp. 1–4.

Sameer Arora (S'14) received the B.Tech. degree in electronics and communication engineering from the Dr. A. P. J. Abdul Kalam Technical University (formerly Uttar Pradesh Technical University), Lucknow, India, in 2008, and the M.S. and Ph.D. degrees in computer engineering from the University of Texas at Dallas, Dallas, TX, USA, in 2012 and 2017, respectively.

His current research interests include dc–dc power converters, power management integrated circuit design, control of power systems, nonlinear control, and their applications.

Dr. Arora is a member of the IEEE Industrial Electronics Society. He has been part of the 2016 IEEE Dallas Circuits and Systems Conference as a committee member. He was a recipient of the Best Paper/Presentation Award at the 2016 Annual Conference of the IEEE Industrial Electronics Society.

Poras T. Balsara (F'14) received the L.E.E. Diploma in electronics from the Victoria Jubilee Technical Institute, Mumbai, India, in 1980, the B.E. degree in electrical engineering from the University of Bombay, Mumbai, in 1983, and the M.S. and Ph.D. degrees in computer science and engineering from the Penn State University, State College, PA, USA, in 1985 and 1989, respectively.

In 1989, he joined the faculty of the Erik Jonsson School of Engineering and Computer Science, University of Texas at Dallas, Dallas, TX, USA, where he is currently a Professor of electrical engineering and the Associate Dean for Academic Affairs. He has authored or coauthored several journals and conference publications and a book. His research interests include very large scale integration design, power electronics, design of energy efficient digital circuits and systems, and digitally assisted mixed-signal design.

Dinesh Bhatia (SM'00) received the Bachelor's degree in electrical engineering from the Regional Engineering College, Suratkal, India, in 1985, and the Master's and Ph.D. degrees in computer science from the University of Texas at Dallas, TX, USA, in 1987 and 1990, respectively.

He is a faculty member at the Erik Jonsson School of Engineering and Computer Science, University of Texas at Dallas, where he directs research activities within the IDEA Lab. He has served on technical program committees of several international conferences related to field-programmable gate arrays (FPGAs), field-programmable technology, and system-level design using FPGAs. His research interests include the system-level design, power and energy systems, and architecture and computer-aided design for FPGAs.

Dr. Bhatia has served on the Editorial Board of the IEEE TRANSACTIONS ON COMPUTERS. He was a Distinguished Lecturer of the IEEE Circuits and Systems Society for 2007–2008.